http://dx.doi.org/10.17159/2411-9717/2018/v118n2a5

Behaviour and fate of uranium in a high-level nuclear waste processing system

by J. Addai-Mensah*† and H. Musiyarira*

Synopsis

Effective control and management of high-level nuclear waste (HLNW) during its hydrothermal processing is crucial to the US Department of Energy's Savannah River tank farm operations. Approximately 130 million dm³ of this 'cold war' legacy waste liquor are stored at site. During processing, sodium aluminosilicate (SAS) polytypes (*e.g.*, amorphous, zeolite, sodalite, and cancrinite) and sodium diuranate waste products enriched in fissionable uranium (U) crystallize, invariably, leading to evaporator fouling and major criticality concern. Fissionable product fouling and its mitigation pose intractable challenges, warranting greater understanding and new knowledge of the underpinning mechanisms. In this paper, some of the tactical investigations into uranium behaviour and interactions with SAS phases in HLNW carried out are reported. It is shown that SAS-mediated co-crystallization of sodium diuranate phase from HLNW liquor at high ionic strength and pH, rather than U ion complex adsorption, largely accounts for the crystallographic destination and presence of U in the plant solid foulant.

Keywords
high-level nuclear waste, sodium diuranate, sodium aluminosilicate, evaporator fouling.

Introduction

Radioactive sodium diuranate formation and fouling in high-level nuclear waste (HLNW) processing plants presents intractable challenges to US 'cold war' legacy waste treatment plants (Hobbs and Edwards, 1994; Oji and Williams, 2002; Addai-Mensah, Li, and Zbic, 2002; Duff, 2002; Addai-Mensah *et al.*, 2005, 2004a, 2004b). Heterogeneous crystallization of sodium diuranate ($Na_2U_2O_7$) occurs in tandem with sodium aluminosilicate phases within the evaporators used in the waste liquor concentration in the temperature range 30–140°C. Typically, the HLNW liquor comprises high ionic strength (6–10 M) caustic solutions containing sodium hydroxide, silicate, aluminate, nitrite, and nitrate ions, trace amounts (approx. 300 mg·dm^{-3}) of radionuclides (*i.e.*, uranium-235, plutonium-238) and radio-toxic species (*e.g.*, caesium-137). The supersaturation of Na ion-paired tetrahydroxo Al(III), SiO_2, and uranyl complex species in solution (the limiting reactants) created by continual water evaporation, together with the intense heating applied, synergistically act to facilitate the poly-condensation and crystallization of SAS and fissionable uranium-based solid products (Hobbs and Edwards, 1994; Puigdomenech and Bruno, 1988; Chernorukov and Kortikov, 2001; Oji Williams, 2002; Duff, 2002; Addai-Mensah *et al.*, 2005, 2004a, 2004 b). The formation and accumulation of SAS involve an amorphous phase and three polytypes: zeolite, sodalite, and cancrinite (Addai-Mensah *et al.*, 1997, 1998, 2001a, 2001 b; Barnes *et al.*, 1999a–f). In the case of the U-based crystalline product, while sodium diuranate is believed to be formed, it is not clear whether other iso-structural U oxide compounds such as $Na(UO_2)_3O_3(OH)_2$ and $Na_6U_7O_{24}$ or the silicate soddyite ($(UO_2)_2SiO_4{\cdot}2H_2O$), are also present. If not effectively mitigated, the accumulation of a critical mass of fissionable U in the scale deposit can (and does) proceed at an alarming rate, posing a major criticality concern and warranting an immediate plant shutdown.

Mechanistically, fouling may occur by a number of ways, including: (i) high surface energy metal substrate-mediated heterogeneous precipitation, (ii) adsorption of existing particulate matter in suspension onto a substrate, (iii) chemical reaction solid product deposition onto an 'inert' substrate, and (iv) substrate corrosion-mediated precipitation product deposition. The mechanisms and kinetics of U-free SAS crystallization and fouling have been investigated under a variety of conditions (Barnes *et al.*, 1999a–f; Addai-Mensah, Lee, and Zbic, 2002; Addai-Mensah *et al.*, 2005, 2004a, 2004b). It can be said that, depending

* *Department of Mining and Process Engineering, Namibia University of Science Technology, Namibia.*

† *Future Industries Institute, University of South Australia, Adelaide, Australia..*

upon the operating conditions, all of the above modes of fouling may prevail. Furthermore, while our fundamental knowledge and understanding of SAS crystallization fouling behaviour have advanced considerably, crucial knowledge of how the actinides' solute species (*e.g.*, weapons-grade uranium and plutonium) present in the HLNW liquor are incorporated into the pervasive SAS scale is limited. This paper presents strategic basic crystallization and U sorption studies carried out to establish the crystallo-chemical characteristics and fouling behaviour of U and SAS solid products in a HLNW simulant system, thus bridging the fundamental knowledge gap.

Experimental methods

Investigations were performed using model simulant liquors and conditions reflecting the US DoE's Savannah River HLNW evaporator processing and fouling behaviour. Synthetic SiO_2-free, sodium aluminate solutions were prepared from known masses of gibbsite (99.5% γ-$Al(OH)_3$, Alcoa Arkansas, USA), sodium hydroxide (97.5% NaOH, 2.5% Na_2CO_3, Ajax Chemicals, Australia), anhydrous sodium carbonate (99.9% Na_2CO_3, Merck, Australia), and Milli-Q water to give a liquor of concentration 2.20–2.33 M $Al(OH)_3$, 5.4–6.0 M NaOH, and 0.49 M Na_2CO_3. A 0.55 dm^3 aliquot of the above liquor was placed in a 1 dm^3 stainless steel autoclave operating at 400 r/min agitation rate at a constant temperature. 0.05 dm^3 solutions containing 0.150–1.50 g of sodium metasilicate (99.9% Na_2SiO_3, Merck, Australia), 0.05 dm^3 of 6.0 M sodium nitrate, and 6.0 M sodium nitrite (99.9% $NaNO_3$ and $NaNO_2$, Merck, Australia) were added to the liquor sequentially once it had reached the required experimental temperature (80–120°C), bringing the total liquor volume to 0.65 dm^3. Known masses of uranyl nitrate ($UO_2(NO_3)_2$) crystals (99.9% pure, Ajax Chemicals, Australia) were dissolved in the final solution to serve as a hexavalent uranium-238 source. The final liquor compositions were 0.01-0.1 M SiO_2, 6.6×10^{-3}-1.2 M $Al(OH)_3$, 0.38 M Na_2CO_3 and 3.8–6.0 M NaOH for U-free liquor type or plus 21–3400 mg·dm^{-3} U, 1.0 $NaNO_3$, and 1.0 $NaNO_2$ for HLNW liquor type. Before use, the solutions were twice filtered through 0.45 μm membranes to give optically clear liquors.

Self-nucleating (unseeded), isothermal crystallization/fouling tests were run over 4 hours at temperatures of 65, 85, and 120°C in a batch autoclave. A 316 stainless steel, high-pressure Parr autoclave fitted with an external heater and an interval cooling system was used. The vessel was fitted with a central four-blade, 45°-pitch, 2-tier impeller which provided constant agitation at 400 ± 2 r/min. The autoclave's temperature, heating, and agitation rates were controlled through an automatic proportional, integral, and derivative control system. To prevent boiling of solution above 100°C, the autoclave was pre-pressurized by using H_2O vapour-saturated N_2 gas to a pressure of 3200 kPa, prior to heating. This also ensured that there was no solution water loss by vapourization. Solution/slurry samples were periodically removed for solution and solid products characterization. 10 × 6 mm 316 stainless steel strips (coupons) screwed onto the shaft of the impeller were detached to routinely provide fouled substrates for standard scanning electron microscopy (SEM), powder X-ray diffraction (XRD), and time-of-flight secondary ion mass spectrometry (ToF SIMS) analyses. The specific surface area of the crystals was determined by N_2 BET analysis (Coulter Omnisorp 100, Hialeah Fl. USA). Solution SiO_2, Al(III), and U concentrations were analysed by ICP-MS (Spectro Analytical Instruments, Spectro SIM-SEQ ICP-OES, Kleve, Germany). The experimental runs were repeated three times for each temperature. Product particle size and size distribution were measured by laser diffraction

SEM analyses of carbon-coated samples were performed using a high-resolution field emission Cam Scan (CS44FF, Cambridge, UK) at 20 or 100 kV in imaging modes secondary electron (SE) and backscattered electron (BSE), and energy dispersive spectroscopy (EDAX) mode for elemental composition. To make BSE imaging of fouled coupons more interpretable, the scale deposit was carefully pressed to render it flat prior to analysis. The solid product/crystalline phase characterization was performed by collecting and analyzing XRD patterns on powder samples in $\theta/2\theta$ scanning mode using CuKα radiation (λ = 1.5418 Å). The scan speed was 1° per minute between 10° and 70° 2θ.

Results and discussion

The kinetic behaviour of self-nucleating solutions crystallizing isothermally over 4 hours was investigated at temperatures of 65, 85, and 120°C. Typical, SEM photomicrographs and EDAX maps of pristine and fouled 316 stainless steel coupons, revealing surface topographical features and elemental composition, are shown in Figures 1–3. Well-defined grain boundaries with asperities can be clearly seen for the pristine steel coupon (Figure 1, X3). Elemental concentrations of Fe, Cr, and Ni as the principal constituents of 316 stainless steel are also indicated in Figure 1.

After heating the U-free, SAS supersaturated liquor (0.01 M SiO_2, 0.12 M $Al(OH)_3$, 0.38 M Na_2CO_3, 1.0 M $NaNO_3$, 1.0 M NO_2, and 4.0 M NaOH) at 85°C for 3 hours, the resulting SEM images and EDAX analyses showed the proliferation of colloidal particles and Na, Al, Si, and O atoms at the steel substrate surface (Figure 2). Common behaviour of SAS polytypes crystallization from U-free Al(III) and SiO_2 supersaturated solutions is depicted in Figure 3 via powder XRD analysis. The identities of the four distinct phases observed at 65–120°C were established as amorphous solid ($Na_{12}Al_{12}Si12O_{48}.27H_2O$), Linde type zeolite A crystals ($Na_{12}Al_{12}Si_{12}O_{48}.27H_2O$) (both dominant at low temperatures <85°C), and dimorphic sodalite and cancrinite crystals (both predominant at higher temperatures > 85°C). The sodalite and cancrinite phases may both be generically described as ($Na_6Al_6Si_6O_{24}Na$ X.$n$$H_2O$) (where $2 \leq n < 4$ and X denotes $2NO_3^-$ and $2NO_2^-$). Both the zeolite A and its amorphous solid precursor contained no detectable amounts of non-framework anionic species in solution (OH^-, CO_3^{2-}, NO_3^-, and NO_2^-) which are characteristic guest species in sodalite and cancrinite structures. The main influence of temperature was observed to be exerted in terms of the kinetics and thermodynamics. The crystallization and phase transformation rates of all four SAS phases increased rapidly with increasing temperature from 65 to 120°C, in the manner of chemical-reaction controlled processes. Typical results obtained in the 65–120°C range are presented herein for 85°C, for brevity. In Figure 3, the temporal, solution-

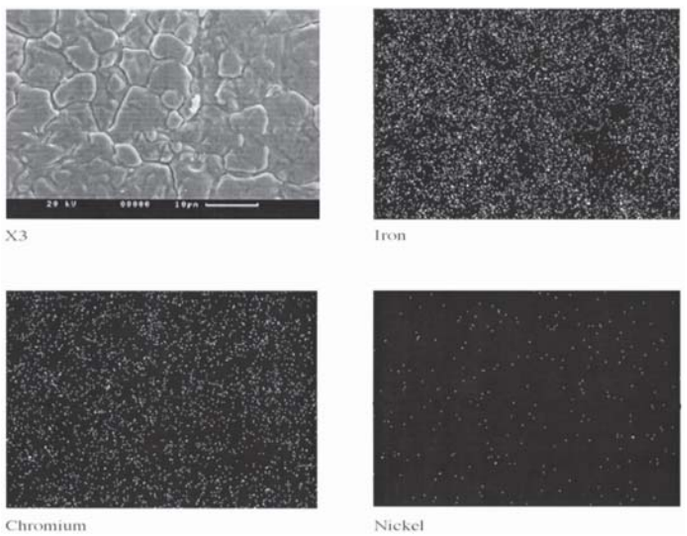

Figure 1—SEM photomicrographs (X3) and EDS maps of pristine 316 stainless steel substrate revealing surface topographical features and elemental composition, respectively

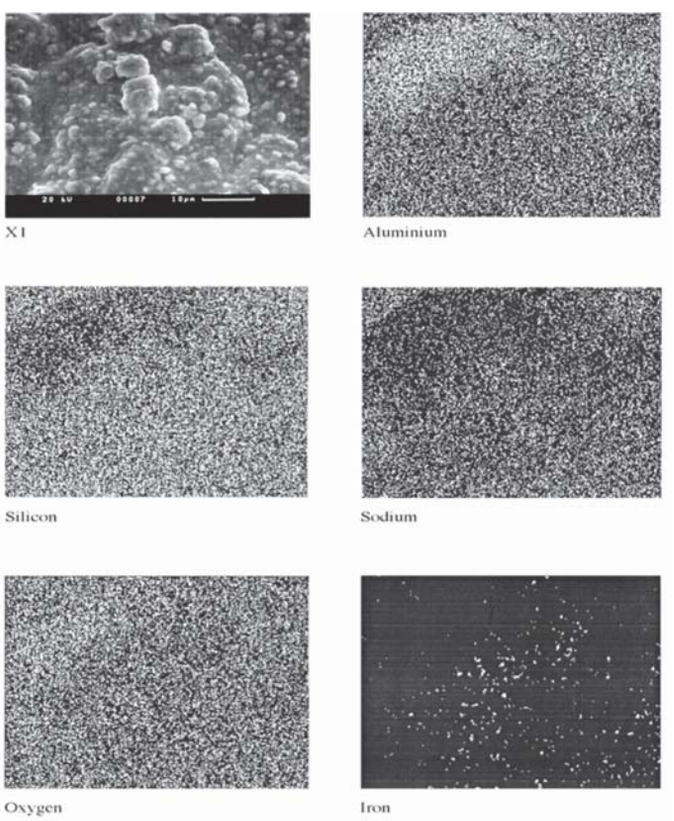

Figure 2—SEM photomicrograph and EDS maps of fouled steel substrate revealing surface topographical features and elemental composition, respectively, during fouling at 85°C from 0.01 M SiO_2, 0.12 M $Al(OH)_3$, 0.38 M Na_2CO_3, 1.0 M $NaNO_3$, 1.0 M NO_2, and 4.0 M NaOH solution

mediated transformation of zeolite A to sodalite and then to cancrinite within 60 minutes at 85°C is exemplified.

To crystallize a U-based solid product while suppressing sodium SAS phase formation, a liquor supersaturated with 3400 mg·dm^{-3} U and containing dissolved Al(III) and SiO_2 at concentrations equivalent to equilibrium solubility of cancrinite, the least soluble SAS phase, was used. The U-based product which crystallized at 65–120°C comprised massively aggregated, polycrystalline, platy and globular particles as the SEM image in Figure 4 shows. The product, crystallized without or with SAS, was established as sodium diuranate ($Na_2U_2O_7$) crystals by powder XRD analysis. The XRD analysis (based on JCPD Standard 12-0106 and data of Kovba, 1972) discounted the presence of other isostructural

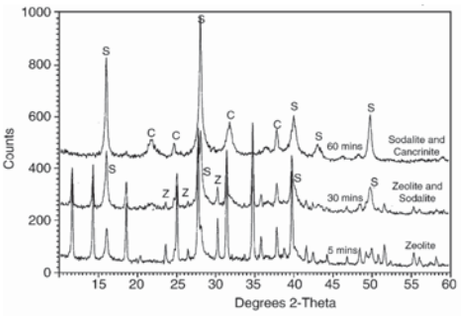

Figure 3—XRD spectra of SAS scale formed within 60 minutes at 85°C from self-nucleating, U-free solution containing 0.01 M SiO_2, 0.12 M $Al(OH)_3$, 0.38 M Na_2CO_3, 1.0 M $NaNO_3$, 1.0 M NO_2, and 4.0 M NaOH

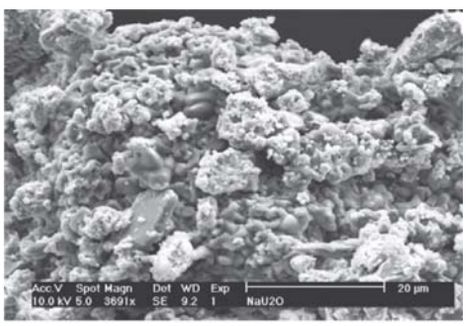

Figure 4—Typical SEM image of precipitated $Na_2U_2O_7$ crystals deposited onto a 316 stainless steel coupon from a self-nucleating, U-supersaturated (and SAS-saturated) liquor at 85°C

uranium oxides phases (*e.g.* $Na(UO_2)_3O_3(OH)_2$ and $Na_6U_7O_{24}$) (Giammar and Hering, 2002; Chernorukov and Kortikov, 2001). To understand the underpinning thermodynamics, the equilibrium solubilities of the $Na_2U_2O_7$ crystals and SAS solid phases in nitrated/nitrited caustic aluminosilicate solutions were determined. Two types of solubility experiments were designed and used to allow the approach to equilibrium from 'above' (via seeded precipitation from supersaturated liquor) and from 'below' (via seeded dissolution in undersaturated liquor) (Addai-Mensah *et al.*, 2004).

Under the conditions used in the present investigation, the equilibrium solubility of the $Na_2U_2O_7$ phase was in the range 9.0–17.0 mg·dm^{-3} U, depending upon solution composition and/or temperature. The solubilities increased with increasing temperature which agreed well with the data reported for U in the literature (Duff, 2002; Hobbs and Edwards, 1994; Puigdomenech, and Bruno, 1988; Cordfunke and Loopstra, 1971) and also for SAS solid products (Zheng *et al.*, 1998; Addai-Mensah *et al.*, 2004; Barnes *et al.*, 1999d, 1999f). The equilibrium solubility (Ce) data was used together with the instantaneous U, Al(III), and SiO_2 species concentrations (Ci) to quantify the species relative supersaturations (σ = Ci/Ce – 1) with crystallization time.

For mixed SAS and sodium diuranate co-crystallization, experiments were conducted under plant-relevant solution and temperature conditions. Typical variations in U, Al(III), and SiO_2 relative supersaturations in self-nucleating solutions with time are shown in Figure 5. The data exemplifies how rapid dissipation of SiO_2, Al(III), and U species supersaturation can proceed when the initial relative supersaturations (σ_0) of SiO_2 and Al(III) > 6 and that of U < 3 sufficiently induce SAS-U nucleation. Following rapid dissipation of supersaturation and prolonged mixed oxide co-precipitation within 2 hours, each of the three limiting reactants asymptotically approaches a plateau value.

SAS-mediated U species desupersaturation was observed, and this was dependent the of U concentration in the liquor. At very high initial U supersaturation (σ_u >10), sodium diuranate crystallization was substantially independent of the rate of SAS co-crystallization. At low relative supersaturations (σ_u) < 2 or U < 40 mg·dm^{-3}, U desupersaturation was insignificant where SAS crystallization did no prevail as a precursor due to low supersaturation. Thus, at close to SAS equilibrium solubility conditions and low U supersaturation, no noticeable U crystallization occurred. Under such conditions, the uptake of U occurs largely by adsorption onto extant SAS solid phases, the extent of which is strongly dependent upon crystal surface area and charge or magma density. At low to moderate U concentration (40–70 mg·dm^{-3}), SAS-U mixed-phase crystallization from supersaturated solutions prevailed. The rate of the mixed SAS and U crystallization followed the sequence: amorphous > zeolite A > sodalite > cancrinite > sodium diuranate. For liquors at low U concentration or supersaturation, SAS nucleation was a necessary precursor for the heterogeneous crystallization of sodium diuranate. The crystallization fouling reactions were observed to be distinctly temperature-dependent and dramatically enhanced at elevated temperatures (> 85°C). The nucleation and growth mechanisms and kinetics were quantified using empirical, second-, and third-order power law models, in the manner of Barnes *et al.* (1999a–d). The activation energies involved the zeolite A, sodalite, and cancrinite crystallization processes were estimated to be in the range 30–120 kJ/mol, the higher and lower values reporting to the concurrent nucleation and crystal growth mechanisms, respectively. The activation energies > 30 kJ/mol are indicative of chemical reaction-controlled crystallization processes.

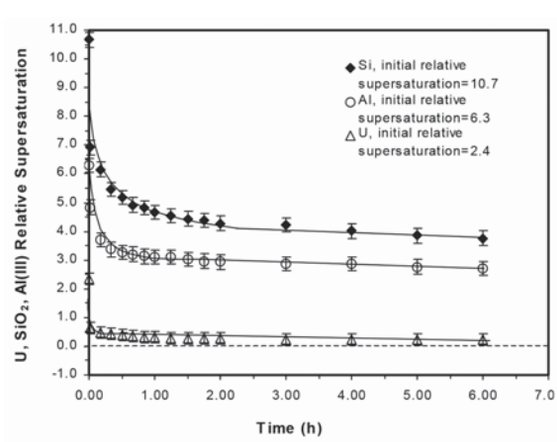

Figure 5—U, SiO_2, and Al(III) relative supersaturations as a function of time during crystallization of U-based oxide and SAS at 85°C (initial solution: NaOH = 4.0 M, $NaNO_3$ = 1.0 M, $NaNO_2$ = 1.0 M, SiO_2(♦)= 175.0 × 10^{-3} M, Al(III) (O) = 175.0 × 10^{-3} M, and U (Δ)= 30.8 mg·dm^3

The heterogeneous scale deposits that crystallized from the U, SiO_2, and Al(III) supersaturated liquors were mixed sodium diuranate and sodium aluminosilicate (amorphous solid, zeolite, sodalite, and cancrinite) phases, as revealed by powder XRD, SEM BSE images, and EDAX analyses. Representative BSE image and EDAX data obtained for U-SAS mixed-phase fouled steel coupon is displayed in Figure 6. For the flat, mixed SAS and U oxide scale deposit prepared and analysed in the present work (*e.g.*, as in Figures 6A and 6B), the BSE images reveal grey and dark regions of high and low signals respectively, which correspond to the highest and lowest average atomic numbers, respectively. These, characteristically, translate into images of U-rich oxide appearing as grey and Al and Si-based oxide as dark areas, as in Figure 6A and EDAX bulk elemental composition analysis (Figures 6B and 6C). It is pertinent to state that the standard analytical techniques (SEM imaging, EDAX, and XRD analyses) employed provided invaluable crystallo-chemical information on the mixed U-SAS oxide scale phases identification and deconvolution.

Surface-sensitive ToF SIMS positive ion spectral analysis was also performed. The image of mixed U-SAS solid phases crystallized onto a steel coupon after 4 hours at moderate U concentration of 70 mg·dm^{-3} (ppm) and 4 M NaOH, 1 M $NaNO_3$, $NaNO_2$, 324 mM Al(III), and 324 mM SiO_2) at 85°C is displayed in Figure 7. The image clearly indicates random spatial distribution of sodium, Al and Si, and U species, which predominate on the surface as expected.

U adsorption studies

In liquors at low U species concentrations (< 40 mg·dm^3) and relative supersaturation ($\sigma < 2$), it was observed that sodium diuranate did not crystallize. In the presence of SAS solid phases in such liquors, adsorption processes are substantially responsible for incorporation of U species into the solid product matrix, the extent of which is dependent upon the SAS polytypes present. The results of the investigations of U adsorption onto the four different SAS solid phases revealed dependency on both substrate type and liquor Al (III) equilibrium concentration. Typical U species adsorption behaviour observed is demonstrated by the data in Figure 8 produced at 85°C for liquor with the following concentration: NaOH 4.0 M, $NaNO_3$ 1.0 M, $NaNO_2$ 1.0 M, SiO_2 1.7–75.0×10^{-3} M, and U 15.0 ppm (mg·dm^{-3}), and SAS seed charge 12 240 m^2·dm^{-3}.

The adsorption loading of U at temperatures < 85°C was highest for the amorphous SAS phase, followed by zeolite A, then sodalite, and the least for the cancrinite phase. In general, U species adsorption loading is remarkably low, accounting for < 5% of the total U species that is incorporated into the mixed SAS-U solids product formed during concentration ofthe HLNW liquor by the evaporation process. Thus, co-crystallization of U species with SAS solid phases is believed to be the main mechanism for the former's appearance in the HLNW evaporator solid product. These observations indicate that heterogeneous nucleation and growth of sodium aluminosilicate phases are critically important mediation processes for U oxide co-precipitation at low to moderate U supersaturations in HLNW evaporators.

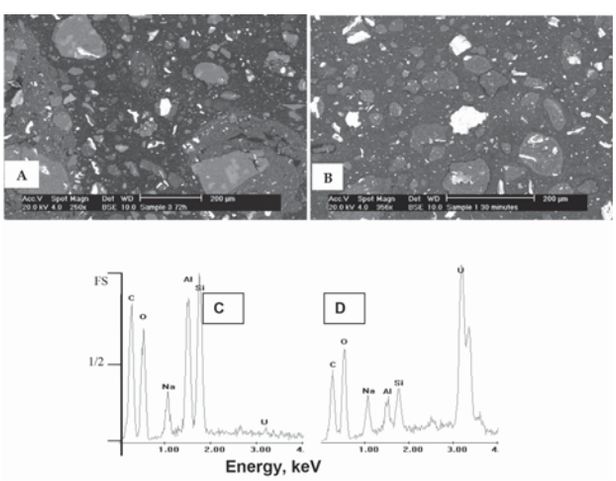

Figure 6—SEM BSE image (A and B) of fouled steel substrates due to co-precipitation of sodium aluminosilicate (dark area) and sodium diuranate (white areas) at 85°C ; EDAX analysis of SAS - region (C) (dark areas in A and B), and sodium diuranate region (D) (white areas in A and B)

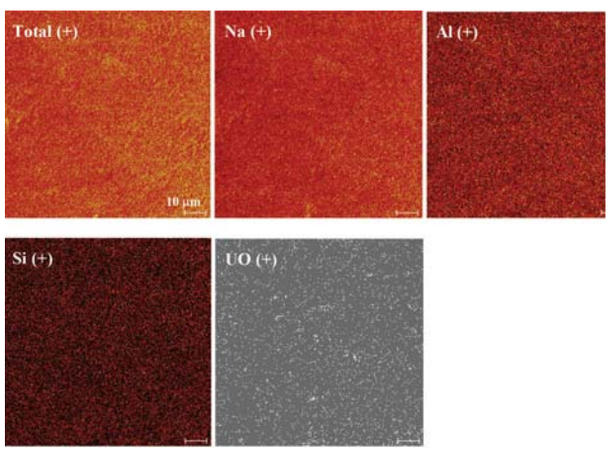

Figure 7—Selected SIMS positive ion images of mixed amorphous NAS- and U-based solid phases precipitated after 4 hours at 85°C from sodium aluminosilicate liquor initially containing 70 mg·dm^{-3} U, 324 mM Al(III), and 324 mM SiO_2. Sodium, Al, and Si (yellow spots) and U species (white points). Note the random distribution of U species at the solid deposite

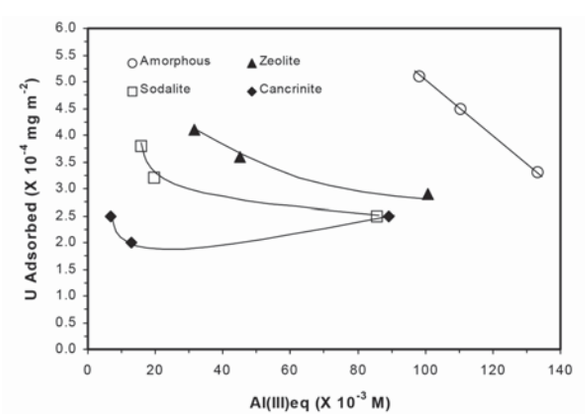

Figure 8—Adsorption loading of U species onto different SAS solid phases as a function of Al(III) equilibrium concentration at 85°C (liquor concentration: NaOH 4.0 M, $NaNO_3$ 1.0 M, $NaNO_2$ 1.0 M, SiO_2 1.7–75.0×10^{-3} M, and U = 15.0 mg·dm^3. Seed charge 12240 m^2·dm^{-3})

Conclusions

Isothermal crystallization and fouling experiments simulating the formation and accumulation of uranium-enriched sodium aluminosilicate scale in the high-level waste evaporators at the US Department of Energy's Savannah River site, were performed. The studies aimed at providing greater understanding and new knowledge of the mechanisms and kinetic behaviour of the processes that determine the fate and crystallographic destination of uranium in the solid product. The analytical characterization of the various products observed under various conditions of liquor supersaturation, saturation, and undersaturation at 60–120˚C revealed the following. Sodium diuranate was the uranium compound that crystallized in the highly caustic and high ionic strength aqueous media, regardless of the operating temperature. This U oxide product formed as both discreet and composite particles with amorphous/gel and crystalline sodium aluminosilicate polytypes (zeolite A, sodalite, and cancrinite) at moderate to high U and SAS supersaturations. The rate of sodium aluminosilicate and mixed U crystallization from supersaturated solutions increased with increasing temperature and followed the sequence of the phases: ephemeral amorphous > zeolite A > sodalite > stable cancrinite > sodium diuranate. For liquors at low U concentration or supersaturation, SAS nucleation was a necessary precursor for heterogeneous crystallization of sodium diuranate. The crystallization fouling reactions are distinctly chemical reaction-controlled, and are dramatically enhanced at elevated temperatures. The findings show that effective management and mitigation of both SAS and U oxide crystallization fouling in process heat-transfer equipment (evaporator) via an appropriate temperature control strategy are of significant importance to the HLNW industry.

Acknowledgments

Financial support for the project from Westinghouse Savannah River Company (Aiken, USA) for this work is gratefully acknowledged. Various contributions and comments made by Drs B. Wilmarth, R. Rosencrance, M. Zbik,, and J. Li are also gratefully acknowledged.

References

Addai-Mensah, J., Li, J. and Zbik, M. 2002. Sodium aluminosilicate solid phases: Chemistry and crystallization behaviour. US Department of Energy–WSRS/ERDA. *Report no*. G008.

Addai-Mensah, J., Li, J., Zbik, M., and Wilmarth, W.R. 2005. Uranium sorption in sodium aluminosilicate phases under caustic conditions. *Separation Science and Technology*, vol. 40, no. 1-3. pp. 267–279.

Addai-Mensah, J., Li, J., Zbik, M., and Rosencrance, S. 2004. Sodium aluminosilicate solid phase specific fouling behaviour. *International Journal of Transport Phenomena*, vol. 6. http://search.ror.unisa.edu.au/record/UNISA_ALMA51109601200001831/media/digital/open/9915913599601831/12143364950001831/13143363950001831/pdf

Addai-Mensah, J., Li, J., Rosencrance, S., and Wilmarth, W.R. 2004. Solubility of amorphous sodium aluminosilicate and zeolite A solid phases in nitrate/nitrite-rich caustic aluminate liquors. *Journal of Chemical and Engineering Data*, vol. 49, no. 6. pp. 1682–1687.

Addai-Mensah, J., Gerson, A.R. Jones, R., and Zbik, M. 2001. Reduction of sodium aluminosilicate scale in Bayer plant heat exchangers. *Light Metals*, vol. 13. pp. 13–18.

Addai-Mensah, J., Barnes, M.C., and Gerson, A.R. 2001. Fouling of alumina refining heat exchangers: Effect of substrate and temperature, *Proceedings of the 6th World Congress of Chemical Engineering, Melbourne Australia*. Institution of Chemical Engineers in Australia, Melbourne. pp. 1–8.

Addai-Mensah, J., Gerson, A.R., O'Dea, A., and Zheng, K. 1997. The precipitation mechanism of sodium aluminosilicate scale in Bayer plants. *Proceedings of Light Metals 1997*, Orlando, FL.. The Minerals, Metals & Materials Society, Warrendale, PA. pp. 23-28.

Addai-Mensah, J., Gerson A.R., and Smart, R.St.C. 1998. Continuous plug flow precipitation of sodalite scale on steel heat transfer surfaces, *Light Metals*, vol. 21. pp. 21–28

Barnes, M.C., Addai-Mensah, J., and Gerson, A.R. 1999a. The kinetics of desilication of synthetic spent Bayer liquor seeded with cancrinite crystals. *Journal of Crystal Growth,* vol. 200, no. 1–2. pp. 251–264.

Barnes, M.C., Addai-Mensah, J., and Gerson, A.R. 1999b. The kinetics of desilication of synthetic spent Bayer liquor seeded with pure sodalite, pure cancrinite and their dimorphic mixed phase crystals. *Light Metals*, pp. 121–130.

Barnes, M.C., Addai-Mensah, J., and Gerson, A.R. 1999c. The kinetics of desilication of synthetic spent Bayer liquor and sodalite crystal growth. *Journal of Colloids and Surfaces A*, vol. 147, no.3. pp. 283–295.

Barnes, M.C., Addai-Mensah, J., and Gerson, A R. 1999d. The mechanism of the sodalite-to-cancrinite phase transformation in synthetic spent Bayer liquors. *Microporous and Mesoporous Materials*, vol. 31, no. 3. pp. 287–302.

Barnes, M.C., Addai-Mensah, J., and Gerson, A.R. 1999e. A methodology for quantifying sodalite and cancrinite phase mixtures and the kinetics of the sodalite to cancrinite phase transformation. *Mesoporous and Macroporous Solids*, vol. 31, no.3. pp. 303–319.

Barnes, M.C., Addai-Mensah, J., Gerson A.R., and Smart, R St.C. 1999f. The solubility of SiO_2 in synthetic spent Bayer liquor seeded with sodalite and cancrinite. *Journal of Colloids and Surfaces A*, vol. 157, no. 1-3. pp. 101–116.

Chernorukov, N.G. and Kortikov, V.E. 2001. $Na[HSiUO_6]$ H_2O: synthesis, structure and properties. *Radiochemistry*, vol. 43, no. 3. pp. 229–232.

Cordfunke, E.G.P, and Loopstra, B.O. 1971. Sodium uranates: preparation and thermochemical properties. *Journal of Inorganic and Nuclear Chemistry*, vol. 33. pp. 2427–2436.

Duff, M.C. 2002. Uranium interactions with sodium aluminosilicates: Part 1 Sorption. US Department of Energy-WSRS. Report no. SRT-LWP-2002-00109.

Giammar, D.E. and Hering, J.G. 2002. Equilibrium and kinetic aspects of soddyite dissolution and secondary phase precipitation in aqueous suspension. *Geochimica et Cosmochim. Acta*, vol. 66, no. 18. pp. 3235–3245.

Hobbs, D.T. and Edwards, T.B. 1994. Solubility of uranium in alkaline salt solutions. US Department of Energy-WSRC. Report TR-93-454.

Kovba, L.M. 1972. Crystal structure of sodium diuranate. *Radiokhimiya*, vol. 14, no. 5. pp. 727–730.

Oji, L.N. and Williams, A. 2002. Incorporation of uranium into sodium aluminosilicate phase. US Department of Energy -WSRST. Report no. SRT-LWP-2002-00109.

O'Connor, D.J., Sexton, B.A., and Smart, R. St.C. eds 2003. Surface Analysis Methods in Materials Science. 2nd edn. Springer, Berlin/New York/London.

Puigdomenech, I. and Bruno, J. 1988. Modeling uranium solubilities in aqueous solutions: validation of a thermodynamic database for the EQ 3/6 Geochemical Codes. SKB, Stockholm. Technical report SKB 88-21.

Zheng, K., Gerson, A.R., Addai-Mensah J., and Smart, R. St.C. 1997. The influence of sodium carbonate on aluminosilicate crystallization and solubility in sodium aluminate solutions. *Journal of Crystal Growth*, vol. 171. pp. 197–208.

Zheng, K., Smart, R.St.C. Addai-Mensah, J., and Gerson, A.R. 1998. Solubility of sodium aluminosilicates in synthetic Bayer liquor. *Journal of Chemical and Engineering Data*, vol. 43, no. 3. pp. 312–317. ◆